metals

MDPI

Article

Formation and Corrosion Resistance of Micro-Arc Oxidation Coating on Equal-Channel Angular Pressed AZ91D Mg Alloy

Aibin Ma [1,2,*], Fumin Lu [1], Qi Zhou [1], Jinghua Jiang [1,*], Dan Song [1,2], Jianqing Chen [1] and Yuxi Zheng [1]

1 College of Mechanics and Materials, Hohai University, Nanjing 210098, China; oski@163.com (F.L.); zhouqhhu@163.com (Q.Z.); songdancharls@hhu.edu.cn (D.S.); chenjq@hhu.edu.cn (J.C.); zhengyuxi3681@163.com (Y.Z.)

2 Suqian Institute, Hohai University, Suqian 223800, China

* Correspondence: aibin-ma@hhu.edu.cn (A.M.); jinghua-jiang@hhu.edu.cn (J.J.); Tel.: +86-25-8378-7239 (A.M. & J.J.); Fax: +86-25-8378-6046 (A.M. & J.J.)

Academic Editors: Vijayaraghavan Venkatesh, Raman Singh and Vinod Kumar
Received: 21 October 2016; Accepted: 2 December 2016; Published: 7 December 2016

Abstract: A commercial AZ91D Mg alloy, after bulk grain refinement by various passes of equal-channel angular pressing (ECAP), was selected for micro-arc oxidation (MAO) in silicate electrolyte, corrosion testing in 3.5 wt % NaCl solution and morphology analyses. The results showed that a large number of ECAP passes resulted in the homogeneous ultrafine-grained (UFG) Mg substrate with broken second-phases. The high-energy defects in the ECAPed samples lowered the anodizing potential of the MAO process, but the partial discharge was severe for those samples below eight passes. Increasing the ECAP pass, the compactness and thickness of the MAO coating first decreased and then increased. Due to the compact coating and the existence of Mg_2SiO_4, the coated alloy with 16 ECAP passes has a lower corrosion rate and a larger R_t value. Besides the well-known strengthening-toughening effect, grain refinement via multi-pass ECAP can improve surface protection of the MAO coating on the UFG Mg alloy.

Keywords: magnesium alloy; bulk grain refinement; ECAP; corrosion resistance; MAO

1. Introduction

Magnesium alloys have received considerable attention in recent years, because of their superior properties such as low density, high strength-to-weight ratio, good electromagnetic shielding and biodegradable properties. However, their application is still limited due to their relatively low strength and poor corrosion resistance [1,2]. The demand for simultaneously improving their strength and corrosion resistance is increasingly becoming the focus of interest of researchers.

Grain refinement via the severe-plastic-deformation (SPD) technique can be expected to markedly improve the strength and the ductility of Mg alloys [3,4]. The most attractive SPD method is equal-channel angular pressing (ECAP), which can result in bulk, homogeneous submicron or nanocrystalline microstructure without reduction of the cross section of the billets [5,6]. Although some ultrafine-grained (UFG) magnesium alloys after multi-pass ECAP exhibit excellent mechanical properties [7], they are more susceptible to corrosion in comparison to the coarse-grained (CG) counterpart [8–10]. Therefore, it is necessary to develop an appropriate surface treatments to protect UFG ECAPed Mg alloys to expand their engineering applications.

Among these surface treatment techniques for the protection of Mg alloys [11–15], anodic oxidation is very popular. Macro-arc oxidation (MAO), as a novel technique developed from traditional anodic oxidation, has attracted more and more attention. It is a low-cost and environmentally-friendly

process, but hardly changes the microstructure and mechanical properties of the treated Mg substrate [16]. MAO coatings have good adhesion to the substrate and high wear resistance but are somewhat porous [17]. Plenty of studies have indicated that properties of MAO coatings are influenced by the nature of metallic substrate, the electrolyte and electric parameters [12,13,18]. However, the effect of various ECAP passes for the grain refinement of Mg substrate on the formation and characterization of MAO coating has not been systematically investigated.

The purpose of this paper is to further investigate the effect of ECAPed Mg substrate with different grain sizes on the characterization and protection of the MAO coating. During the repetitive ECAP at the setting temperature, the pass number is the main factor to control the microstructure evolution of the ECAP billet. As is well known, AZ91 alloy is one of the most commonly used Mg alloys in the automotive field. Herein, four kinds of the ECAPed AZ91D samples for up to 16 passes were coated in the same MAO conditions and then immersed in 3.5 wt % NaCl solutions at room temperature. Optical microscopy (OM) and scanning electron microscopy (SEM) were used to characterize the structure and thickness of the formed MAO coatings. The effectiveness of the MAO coating on corrosion protection of the ECAPed Mg alloy was investigated by electrochemical measurements. The results would be helpful for combining the ECAP and MAO processes to obtain the bulk UFG AZ91D alloy with good mechanical properties and corrosion resistance.

2. Materials and Methods

A commercial AZ91D alloy cast ingot, which contains about 9.05 mass % Al, 0.65 mass % Zn, 0.21 mass % Mn and Bal. Mg, was used to prepare bulk fine-grained samples by repetitive ECAP processing. The multi-pass ECAP procedure was conducted at 523 K through route A, using a rotary-die with a channel angle of 90° [19]. The billets with dimensions of 19.5 mm × 19.5 mm × 40 mm were continuously pressed for various passes to obtain the uniformly distributed and UFG microstructure. Four kinds of AZ91D samples with various ECAP passes (4, 8, 12 and 16, respectively) were applied to investigate the effect of the fine-grained Mg substrate on the formation and corrosion resistance of the MAO coating.

A MAO-60 micro-arc oxidation system was used to synthesize the MAO coating on the ECAPed AZ91D samples and the as-cast CG counterpart. Cubical samples (with dimensions of 10 mm × 10 mm × 10 mm) cut from the core of the ECAPed billets were used as the working electrodes (anode), while two parallel stainless steel plates were used as the counter electrodes (cathode). Before the MAO process, all the samples were ground to a grit of 1200 by SiC papers, followed by degreasing in acetone and rinsing in ethanol. The alkaline electrolyte was prepared from distilled water containing 18 g/L sodium silicate, 8 g/L sodium hydroxide, 10 g/L potassium fluoride, 10 g/L glycerol and 5–10 g/L borax. During the MAO process, the temperature of the electrolyte was kept at 293 K. A constant voltage of about 350 V on the samples was maintained for 20 min using a pulse power supply. The frequency and duty cycle were fixed at 500 Hz and 20%, respectively. After the MAO process, the obtained oxide coatings on the CG and UFG Mg substrates were rinsed in distilled water, dried in hot air and kept in a drying chamber for tests.

The microstructure of the samples with and without MAO was observed by an optical microscope (BX51M, Olympus, Tokyo, Japan) and a scanning electron microscope (S340-N, Hitachi, Tokyo, Japan). The ECAPed AZ91D samples for OM or SEM observation were cut perpendicular to the pressing direction, polished by distilled water and etched by the solution containing 2.5 mL acetic acid, 3 g picric acid, 50 mL ethyl alcohol and 5 mL distilled water. The porosity of the MAO coating was detected by Image-Pro Plus 6.0 and estimated from the surface SEM morphology. The phase compositions of the MAO coatings were detected by an X-ray diffractometer (XRD, D8 Advance, Bruker, Karlsruhe, Germany) with Cu Kα radiation and the detected angle (2θ) was scanned from 20° to 90° at a speed of 2°/min.

All MAO samples subjected to corrosion tests were covered by epoxy resins leaving an exposed area of 1 cm^2. Mg alloy is sensitive to pitting corrosion, especially in an electrolyte containing Cl^- ion.

Thus, a conventional 3.5 wt % NaCl aqueous solution (pH = 7) was used for corrosion tests. All the tests were performed twice to ensure the reproducibility of the results. Immersion tests were carried out at room temperature for 12 days in an open system. The initial MAO samples were first cleaned according to the procedure of ASTM standard G-I-72 [20]. After the set intervals of immersion, the mass loss of the samples was examined by AL204 electronic balance (accuracy: 0.1 mg) to calculate the corrosion rate (unit: $mg \cdot cm^{-2} \cdot h^{-1}$) of the coated AZ91D alloy. Electrochemical impedance (EIS) tests were conducted using a PARSTAT 2273 advanced potentiostat (Ametek, Berwyn, IL, USA) equipped with a reference electrode Hg–Hg_2Cl_2/saturated KCl (SCE), Pt counter electrode and Luggin capillary. The frequency of EIS tests ranged from 10 mHz to 10 KHz, and the amplitude of the sinusoidal potential signal was 20 mV with respect to the open circuit potential of the samples.

3. Results and Discussion

3.1. Microstructure Observation of the ECAPed AZ91D Alloy

Figure 1 presents micrographs of the ECAPed AZ91D alloy with various passes. Ternary Mg–Al–Zn alloys, with the Al/Zn ratio of larger than 3:1, generally consist of a hexagonal-close-packed-structure solid solution (the α-Mg phase with Al) and an intermetallic compound (the β-phase with a stoichiometric composition of $Mg_{17}Al_{12}$) [21]. The typical microstructure of the as-cast AZ91D alloy (Figure 1a) was characterized by the presence of the primary α-Mg phase and the divorced eutectic β-phase ($Mg_{17}Al_{12}$) distributed along the α-Mg phase grain boundaries. It can be seen that the initial CG microstructure was severely deformed after multi-pass ECAP. With the ECAP pass increasing, the primary α-Mg matrix and the divorced eutectic along α-Mg grain boundaries were distorted and elongated with the plastic flow along the shear direction. Meanwhile, the continuous and coarse β phase along the α-Mg grain boundaries was gradually stretched, broken and refined because of severe shear strain (imposed about 1.1 after one pass [22]). Those imposed strains during repetitive ECAP also led to many crystalline defects (such as grain boundaries and intragranular dislocation). After ECAP for 12 passes, the sample had a homogeneous, fine-grained microstructure with homogeneously distributed and small β-phase particles. After ECAP for 16 passes, the grain size of the α-Mg matrix decreased from 200 μm to 1–2 μm and the ultra-fined microstructure was obtained. Meanwhile, the original coarse net-like β-phases (as shown in Figure 1a,b) were completely refined to smaller particles with the size of approximate 7 μm and homogenously distributed in the UFG α-phase matrix (Figure 1e). Our previous TEM investigation presents a more detailed microstructure characterization of the UFG AZ91D alloy after 12 ECAP passes [9]. The ultrafine grains were divided into smaller subgrains while abundant dislocations were stored in the deformed grains. During the multi-pass ECAP process, the dislocations would continuously evolve into dislocation tangles, dislocation cells, dislocation walls and sub-grain boundaries, finally forming new grain boundaries to create new, refined, fine grains with high-angle grain boundaries (HAGBs). The mass of dislocations and HAGBs in the UFG AZ91D alloy, acting as the fast atomic diffusion channels [23], can make its chemical activity higher than that of the as-cast alloy.

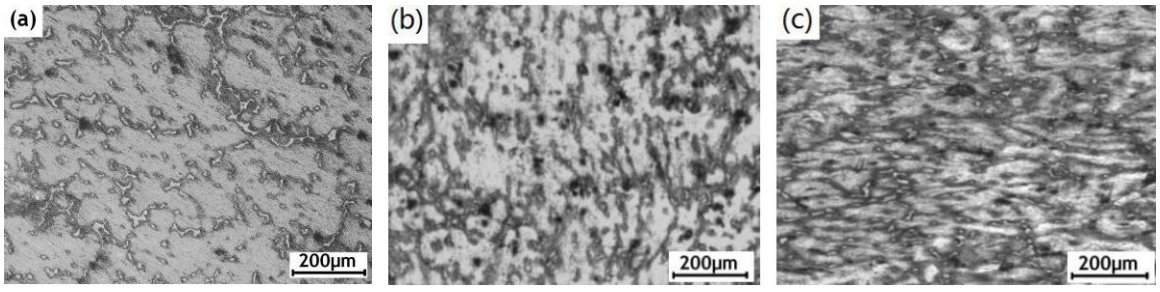

Figure 1. *Cont.*

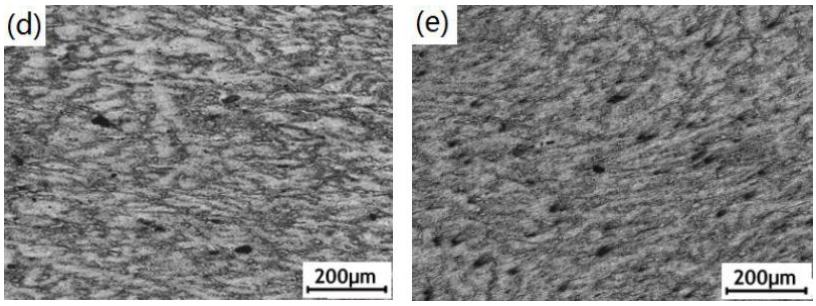

Figure 1. Micrographs of the AZ91D alloy before and after multi-pass equal-channel angular pressing: (**a**) as-cast; (**b**) 4 passes; (**c**) 8 passes; (**d**) 12 passes and (**e**) 16 passes.

3.2. Formation and Morphologies of the MAO Coatings

The MAO process revealed that the breakdown and micro-arc anodizing potentials of the UFG AZ91D sample via multi-pass ECAP were lower than those of the as-cast sample. The lower potential values mean that the driving force of the MAO coating on the UFG substrate was raised, because a large number of high-energy defects were formed in the multi-pass ECAP process [9]. The uniform micro-arc discharge was also found on the UFG AZ91D alloy above 12 passes, but severe partial discharge was observed on the surface of the as-cast sample and those samples below eight passes. The analysis of XRD (Figure 2) indicated that MgO was the main phase of the MAO coating and Mg_2SiO_4 existed in the coating of the 12-pass and 16-pass samples. It can be seen that the ECAP pass increasing makes the MAO formation easy and leads to a complex coating.

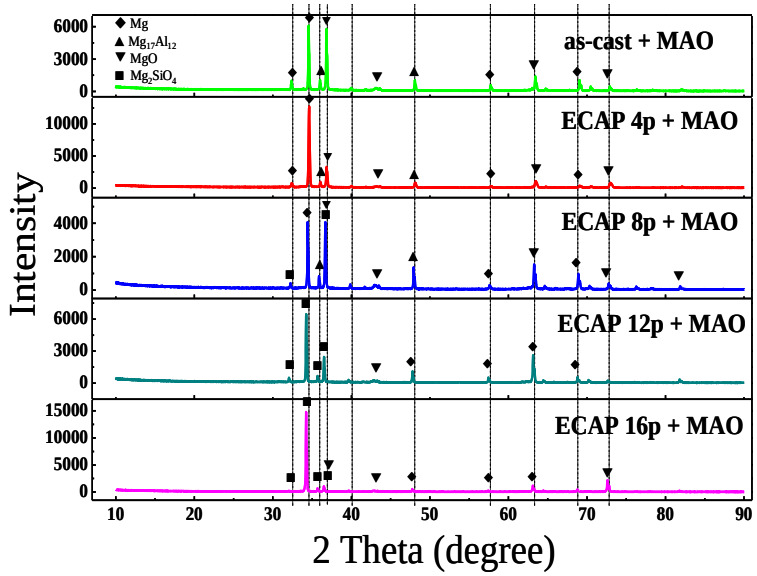

Figure 2. X-ray diffraction patterns of micro-arc oxidation on the as-cast and ECAPed AZ91D magnesium alloys.

Figure 3 presents surface morphologies of the MAO coated on the as-cast AZ91D alloy and the ECAPed ones with various passes. Many randomly distributed micro-pores were observed on the coating, which average diameter ranges from 1 to 5 μm. The existence of micro-pores is a common characteristic of the MAO coating. These micro-pores were formed by the molten oxides and gas bubbles thrown out of micro-arc discharge channels [13]. Because micro-arc discharge always occurred on the relatively weak position [24,25], the micro-pores were considered not to penetrate the Mg substrate. It was also seen that the micro-pores of the MAO coating on the ECAPed alloy had a bigger

average size in comparison with those on the as-cast sample. Moreover, some micro-cracks were observed on the surface of the MAO coating formed on the 8-pass sample, which may weaken the protective effect of the coating. The occurrence of micro-cracks is associated with the high residual stress of the 8-pass sample, and thus there are no cracks on the coating of the AZ91 samples with fewer ECAP passes. The coated samples with more than eight ECAP passes are also not liable to crack, indicating that the complex coatings with the Mg_2SiO_4 phase are more compact and uniform.

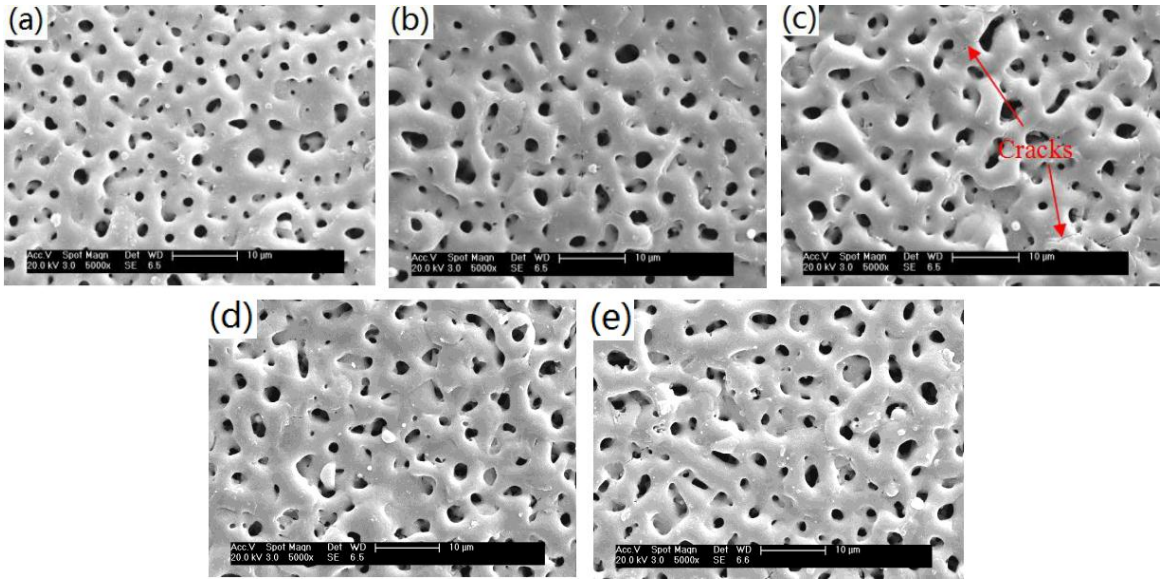

Figure 3. SEM images of the surface of the micro-arc oxidation coatings on (**a**) the cast AZ91D alloy and the ECAPed ones at 523 K for (**b**) 4 passes; (**c**) 8 passes; (**d**) 12 passes and (**e**) 16 passes.

Uniform size and distribution of micro-pores of the coated UFG AZ91D sample surface may result from the finer discharge sparking in the MAO processing. Under the high electric field and Joule heat, the α-Mg phase can release more Mg^{2+} to form the MAO coating but the local discharge on the coarse β-phase was so severe as to form large micro-pores [26]. After 16 ECAP passes, the UFG microstructure with homogeneous and fine β-phase particles made the discharge sparking extremely fine and micro-pores uniform. Furthermore, the broken β-phase particles were beneficial to the elimination of the unclosed holes. It suggests that the uniform and compact MAO coating can be formed on the UFG AZ91D alloy, and thus protect the Mg matrix from corrosion more effectively.

Figure 4 presents cross-sectional morphologies of the MAO coatings on the AZ91D alloy with various passes of ECAP. It is obvious that the MAO coating on the AZ91D samples is composed of a compact inner layer and a porous outer layer. The inner layer (about 1–2 μm) acting as a barrier was formed at the initial discharge, sparking when the voltage increased above the breakdown potential [27]. The thickness of the porous outer layer is greater than that of the compact inner layer. With the ECAP passes increasing, the compactness and thickness of the MAO coating first decreased and then increased. The thickness of the MAO coating formed on the as-cast alloy was nearly equal to that of the 16-pass one, but the outer layer of the coating formed on the UFG AZ91D alloy was more compact and exhibited a better bonding with the matrix. The compact MAO coating was beneficial to raise the corrosion resistance of the coated sample [28].

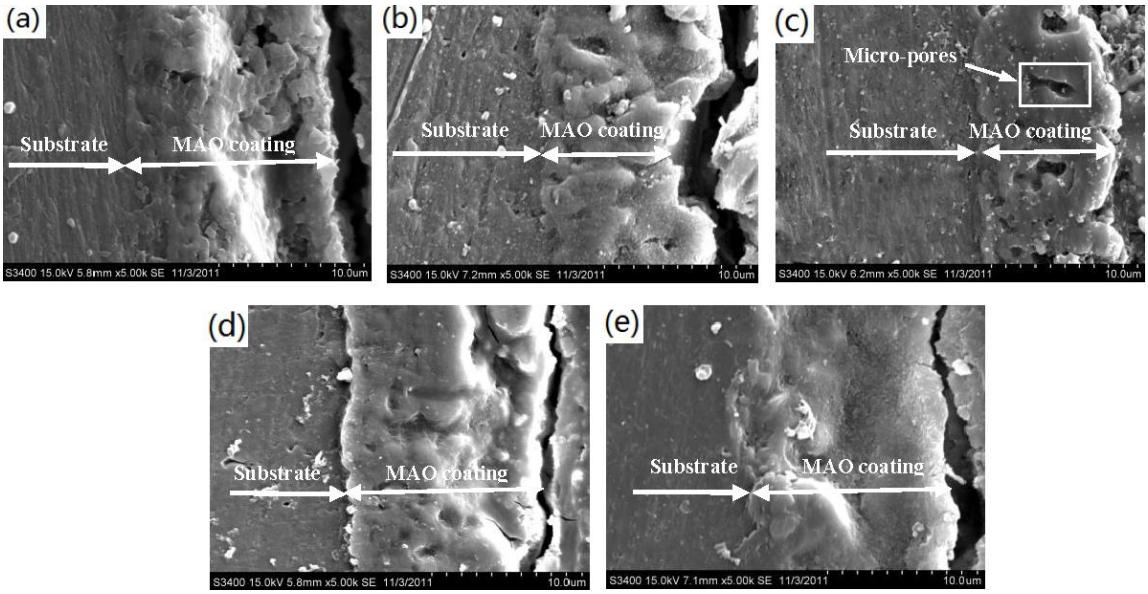

Figure 4. SEM images of the cross-section morphology of the MAO coatings on (**a**) cast AZ91D alloy and ECAPed AZ91D alloys at 523 K with (**b**) 4 passes; (**c**) 8 passes; (**d**) 12 passes and (**e**) 16 passes.

3.3. Corrosion Behavior in the Constant Immersion Test

Figure 5 illustrates the mass loss of the coated samples during immersion in 3.5% NaCl solution. At the initial immersion stage (about 1–2 d), the mass of each sample increases and the mass gain of the 8-pass sample is biggest. It results from the adhesion of corrosion products on the wall side of the micro-pores in the MAO coating. The existence of corrosion products can prevent the Mg substrate from direct contact with the electrolyte through the unclosed micro-pores. At the following stable stage (2–6 d), the formation rate of corrosion products and the solution rate of the MAO coating was approximately similar. After immersion for about 7 days, the mass loss happened because the MAO coating and the matrix were corroded. With the increase of immersion time, the coating and corrosion product exfoliated from the samples. During the whole immersion testing, the corrosion rate of the MAO coating on UFG AZ91D is lower than that of the as-cast sample. This indicates that the MAO coating on the UFG AZ91D alloy has better corrosion resistance and protection.

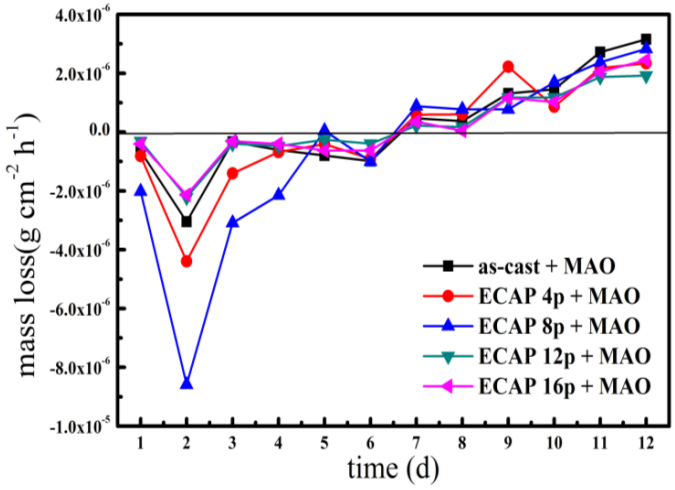

Figure 5. Relationship between the mass loss and the immersion time of the MAO samples in 3.5 wt % NaCl solution.

Macro observation of the coated samples shows that the MAO coatings are still, even with few local damages after immersion in 3.5 wt % NaCl solution for 4 days. Increasing the ECAP pass of the Mg substrate, the corrosion form of the coated sample was changed from pitting corrosion to uniform corrosion. Figure 6 presents SEM morphologies of the local broken MAO coatings on the as-cast alloy and the ECAPed samples after immersion in 3.5 wt % NaCl solution for 4 days. Severe corrosion pits can be found on the as-cast, 4-pass and 8-pass samples. These pits can make the electrolyte penetrate the Mg substrate under the corroded MAO coating and accelerate the corrosion of the coated samples due to the large cathode (the non-erosion coating)-small anode (the corroded area) combination. Different to the other samples, the MAO coating on the 16-pass AZ91D sample shows more uniform corrosion morphology. No obvious pits can be found on the surface of the coated 16-pass sample, which can be attributed to the higher compactness and thickness of the MAO coating (Figure 4e).

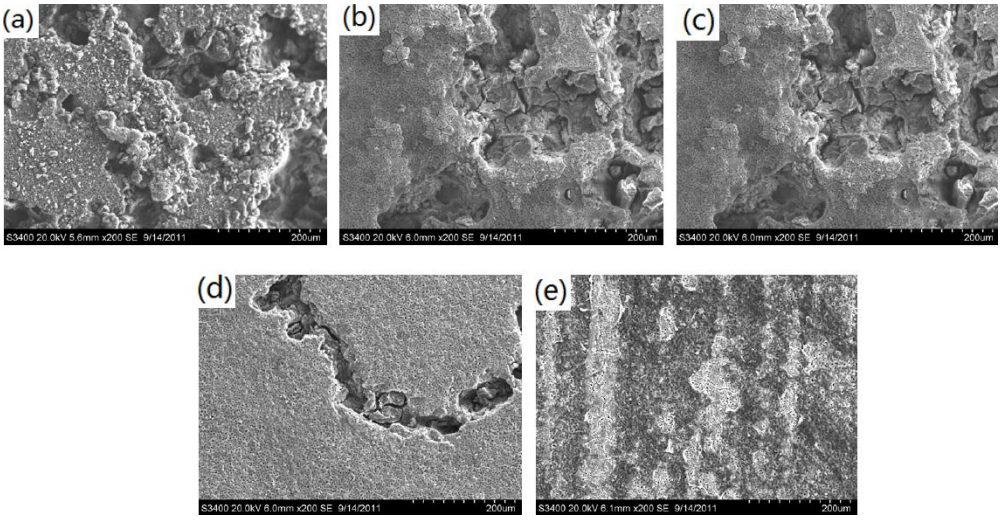

Figure 6. SEM morphologies of the broken MAO coatings on the as-cast and ECAPed AZ91D samples immersed in 3.5 wt % NaCl solution for 4 days: (**a**) as-cast; (**b**) 4 passes; (**c**) 8 passes; (**d**) 12 passes and (**e**) 16 passes.

Figure 7 shows optical morphologies of the coated samples which were immersed in 3.5 wt % NaCl solution for 12 days. It is obvious that the MAO coatings were completely corroded after immersion for 12 days. Without the protection of the MAO coating, the as-cast sample presents the typical pitting morphology. The severe local corrosion happened to the coated samples with four and eight passes of ECAP. The MAO coating on the UFG 16-pass AZ91D alloy is rather effective at protecting the Mg matrix due to its uniform and compact structure. Besides the well-known strengthening-toughening effect, a large number of ECAP passes also can change localized corrosion to general corrosion and increase surface protection of the MAO coatings on the UFG Mg alloy with broken second-phase particles.

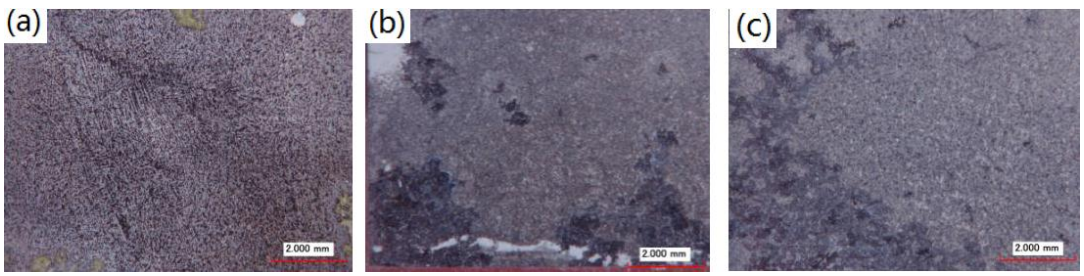

Figure 7. *Cont.*

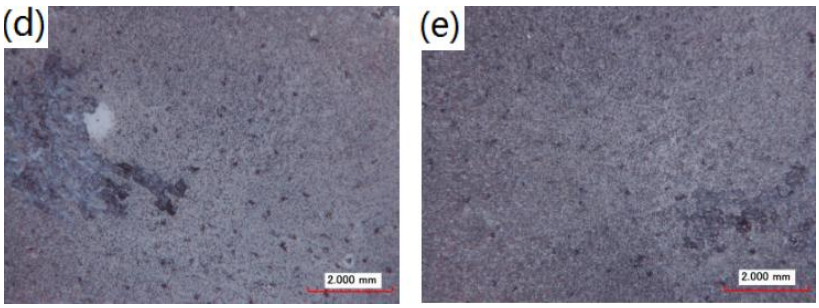

Figure 7. Macro-morphologies of the coated samples immersed in 3.5 wt % NaCl solutions for 12 days: (**a**) as-cast; (**b**) 4 passes; (**c**) 8 passes; (**d**) 12 passes and (**e**) 16 passes.

3.4. Electrochemical Corrosion Behaviors

Figure 8 shows Nyquist plots of impedance spectra of the MAO coatings formed on the as-cast AZ91D and the ECAPed ones after immersion in 3.5 wt % NaCl solutions for 30 min and 1 day, respectively. In the initial immersion time (about 30 min), the capacitive-arc diameters of the ECAPed AZ91D alloy for 12 and 16 passes are much larger than that of the as-cast sample. It indicates that the MAO coating formed on the ECAPed Mg substrate is more corrosion resistant than that on the as-cast sample in the initial immersion period. It is obvious that the capacitive-arc diameter of the ECAPed AZ91D increases as the ECAP pass is increased. After immersion for 1 day, capacitive-arc diameters of all samples decreased and an obvious inductive loop appeared, implying the pitting occurrence [29]. The lower capacitive-arc diameter means that the coating corrosion becomes more severe due to the pitting occurrence. The capacitive-arc diameter of the UFG AZ91D with 16 passes was still larger than the as-cast sample, showing that the MAO coating on the UFG AZ91D has better corrosion resistance. Although the corrosion resistance of the coated sample with fewer passes is lower than that of the as-cast sample, the sample with a large number of ECAP passes is more corrosion resistant than the as-cast sample.

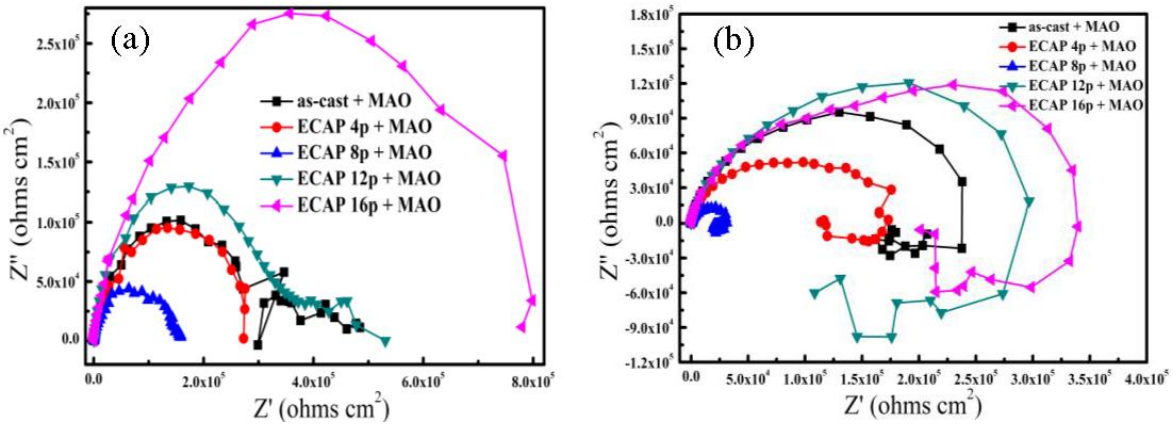

Figure 8. Nyquist plots of impedance spectra of the coated AZ91D samples immersed in 3.5 mass % NaCl solutions for (**a**) 30 min and (**b**) 1 day.

This fact indicates that the MAO structure and the corrosion resistance of the coated AZ91D sample are mainly affected by the microstructure of the alloy substrate. The MAO coating on the UFG alloy substrate is more compact, and thus more anti-corrosive than that on the as-cast CG sample. Our previous investigation indicated that various kinds of non-equilibrium and high-energy defects (such as the sub-grain boundaries and dislocation) showed up during the warm ECAP process [20]. Those crystal defects can act as fast atomic diffusion channels to enhance the chemical

activity of the UFG alloy [23]. Thus, the driving force of the MAO process was raised for the UFG sample, and promoted the formation of the more compact and thicker coating. For the coated UFG alloy, the compact outer layer can more effectively protect the substrate from corrosion. Therefore, the anti-corrosion enhancement of the coated UFG alloy is more marked than that of the coated CG one.

4. Conclusions

The compact MAO coating with uniform size and distribution of micro-pores can be formed on the UFG AZ91D alloy, fabricated by the multi-pass ECAP procedure, attributed to the homogenous micro-arc discharge during the MAO process. The high-energy defects stored in the ECAPed AZ91D alloy also raise the driving force to form the MAO coating, and thus make the coatings on the UFG Mg alloy more compact and thicker. The MAO process with suitable process parameters has a great potential in surface protection of the UFG AZ91D alloy with excellent mechanical properties. After immersion in 3.5 wt % NaCl solution, the MAO coating on the ECAPed AZ91D alloy has a lower corrosion rate and a larger R_t value than that on the coarse-grained as-cast sample. General corrosion happened on the coated alloy with the UFG Mg matrix and fine β-phase particles. Besides the well-known strengthening-toughening effect, bulk grain refinement in advance makes the coated AZ91D alloy more corrosion resistant.

Acknowledgments: This work is financially supported by the Fundamental Research Funds for the Central Universities (Grant No. HHU2016B10314), the Research Innovation Program for Graduate students of Jiangsu Province of China (Grant No. 2010-278), Qing Lan Project and Six Major Talent Peaks Project of Jiangsu Province of China (Grant No. 2014-XCL-023).

Author Contributions: The work presented here was carried out in collaboration between all authors. Aibin Ma and Jinghua Jiang defined the research theme. Qi Zhou and Fumin LU designed methods and experiments, carried out the laboratory experiments, analyzed the data, interpreted the results and wrote the paper. Dan Song, Jianqing Chen and Yuxi Zheng co-designed experiments, discussed analyses and interpretation. All authors have contributed to, seen and approved the manuscript. The author hopes that this paper can make its due contribution to the successful application and protection of the high-performance ultrafine-grained Mg alloy via ECAP.

Conflicts of Interest: The authors declare no conflict of interest.

References

1. Mordike, B.L.; Ebert, T. Magnesium properties-applications-potential. *Mater. Sci. Eng. A* **2001**, *302*, 37–45. [CrossRef]
2. Chang, L.R.; Cao, F.H.; Cai, J.S.; Liu, W.J.; Zhang, Z.; Zhang, J.Q. Influence of electric parameters on MAO of AZ91D magnesium alloy using alternative square-wave power source. *Trans. Nonferr. Met. Soc. China* **2011**, *21*, 307–316. [CrossRef]
3. Yuan, Y.C.; Ma, A.B.; Gou, X.F.; Jiang, J.H.; Song, D.; Zhu, Y.T. Superior mechanical properties of ZK60 mg alloy processed by equal channel angular pressing and rolling. *Mater. Sci. Eng. A* **2015**, *630*, 45–50.
4. Máthis, K.; Gubicza, J.; Nam, N.H. Microstructure and mechanical behavior of AZ91 Mg alloy processed by equal channel angular pressing. *J. Alloy. Compd.* **2005**, *394*, 194–199. [CrossRef]
5. Stolyarov, V.V.; Zhu, Y.T.; Alexandrov, I.V.; Lowe, T.C.; Valiev, R.Z. Grain refinement and properties of pure Ti processed by warm ECAP and cold rolling. *Mater. Sci. Eng. A* **2003**, *343*, 43–50. [CrossRef]
6. Shin, D.H.; Kim, I.; Kim, J.; Kim, Y.S.; Semiatin, S.L. Microstructure development during equal-channel angular pressing of titanium. *Acta Mater.* **2003**, *51*, 983–996. [CrossRef]
7. Chen, B.; Lin, D.; Jin, L.; Zeng, X.; Lu, C. Equal-channel angular pressing of magnesium alloy AZ91 and its effects on microstructure and mechanical properties. *Mater. Sci. Eng. A* **2008**, *483–484*, 113–116. [CrossRef]
8. Minárik, P.; Král, R.; Janeček, M. Effect of ECAP processing on corrosion resistance of AE21 and AE42 magnesium alloys. *Appl. Surf. Sci.* **2013**, *281*, 44–48. [CrossRef]
9. Song, D.; Ma, A.B.; Jiang, J.H.; Lin, P.H.; Yang, D.H.; Fan, J.F. Corrosion behavior of bulk ultra-fine grained AZ91D magnesium alloy fabricated by equal-channel angular pressing. *Corros. Sci.* **2011**, *53*, 362–373. [CrossRef]

10. Li, X.; Jiang, J.H.; Zhao, Y.H.; Ma, A.B.; Wen, D.J.; Zhu, Y.T. Effect of equal-channel angular pressing and aging on corrosion behavior of ZK60 magnesium alloy. *Trans. Nonferr. Met. Soc. China* **2015**, *25*, 3909–3920. [CrossRef]
11. Fan, X.Z.; Wang, Y.; Zhou, B.L.; Gu, L.J.; Huang, W.Z.; Cao, X.Q. Preparation and corrosion resistance of MAO/Ni–P composite coat on Mg alloy. *Appl. Surf. Sci.* **2013**, *277*, 272–280. [CrossRef]
12. Zhang, Y.J.; Yan, C.W.; Wang, F.H.; Lou, H.Y.; Cao, C. Study on the environmentally friendly anodizing of AZ91D magnesium alloy. *Surf. Coat. Technol.* **2002**, *161*, 36–43. [CrossRef]
13. Laleh, M.; Kargar, F.; Rouhaghdam, A.S. Formation of a compact oxide layer on AZ91D magnesium alloy by microarc oxidation via addition of cerium chloride into the MAO electrolyte. *J. Coat. Technol. Res.* **2011**, *8*, 765–771. [CrossRef]
14. Chen, C.Z.; Dong, Q.; Wang, D.G. Microstructure and element distributions of ceramic-like coatings on the AZ91 alloy by micro-arc oxidation. *Surf. Rev. Lett.* **2006**, *13*, 63–68. [CrossRef]
15. Krishna, L.R.; Poshal, G.; Sundararajan, G. Influence of electrolyte chemistry on morphology and corrosion resistance of micro arc oxidation coatings deposited on magnesium. *Metall. Mater. Trans. A* **2010**, *41*, 3499–3508. [CrossRef]
16. Jin, F.; Chu, P.; Xu, G.; Zhao, J.; Tang, D.; Tong, H. Structure and mechanical properties of magnesium alloy treated by micro-arc discharge oxidation using direct current and high-frequency bipolar pulsing modes. *Mater. Sci. Eng. A* **2006**, *435–436*, 123–126.
17. Chen, J.; Zeng, R.C.; Huang, W.J.; Zheng, Z.Q.; Wang, Z.L.; Wang, J. Characterization and wear resistance of macro-arc oxidation coating on magnesium alloy AZ91 in simulated body fluids. *Trans. Nonferr. Met. Soc. China* **2008**, *18*, S261–S364. [CrossRef]
18. Jiang, J.; Zhou, Q.; Yu, J.; Ma, A.; Song, D.; Lu, F.; Zhang, L.; Yang, D.; Chen, J. Comparative analysis for corrosion resistance of micro-arc oxidation coatings on coarse-grained and ultra-fine grained AZ91D Mg Alloy. *Surf. Coat. Tech.* **2013**, *216*, 259–266.
19. Song, D.; Ma, A.; Jiang, J.; Lin, P.; Yang, D.; Fan, J. Corrosion behavior of equal-channel-angular-pressed pure magnesium in NaCl aqueous solution. *Corros. Sci.* **2010**, *52*, 481–490. [CrossRef]
20. American Society for Testing and Materials International. *G31, Recommended Practice for Laboratory Immersion Corrosion Testing of Metals*; Annual Book of ASTM Standards; ASTM: West Conshohocken, PA, USA, 1977; p. 722.
21. Malik, K.N.B. Discontinuous and continuous precipitation in magnesium-aluminium type alloys. *J. Alloy. Compd.* **2009**, *477*, 870–876. [CrossRef]
22. Segal, V.M. Materials processing by simple shear. *Mater. Sci. Eng. A* **1995**, *197*, 157–164.
23. Tong, W.P.; Tao, N.R.; Wang, Z.B.; Lu, J.; Lu, K. Nitriding iron at lower temperatures. *Science* **2003**, *299*, 686–688. [CrossRef]
24. Wang, Y.Q.; Zheng, M.Y.; Wu, K. Microarc oxidation coating formed on SiCw/AZ91 magnesium matrix composite and its corrosion resistance. *Mater. Lett.* **2005**, *59*, 1727–1731. [CrossRef]
25. Apelfeld, A.V.; Bespalova, O.V.; Borisov, A.M.; Dunkin, O.N.; Goryaga, N.G.; Kulikauskas, V.S.; Romanovsky, E.A.; Semenov, S.V.; Souminov, I.V. Application of the particle backscattering methods for the study of new oxide protective coatings at the surface of Al and Mg alloys. *Nucl. Instrum. Methods Phys. Res. B* **2000**, *161–163*, 553–557.
26. Song, Y.L.; Liu, Y.H.; Yu, S.R.; Zhu, X.Y.; Wang, Q. Plasma electrolytic oxidation coating on AZ91 magnesium alloy modified by neodymium and its corrosion resistance. *Appl. Surf. Sci.* **2008**, *254*, 3014–3020. [CrossRef]
27. Wang, Y.; Wang, J.; Zhang, J.; Zhang, Z. Characteristics of anodic coatings oxidized to different voltage on AZ91D Mg alloy by micro-arc oxidization technique. *Mater. Corros.* **2005**, *56*, 88–92. [CrossRef]
28. Duan, H.P.; Yan, C.W.; Wang, F.H. Effect of electrolyte additives on performance of plasma electrolytic oxidation films formed on magnesium alloy AZ91D. *Electrochim. Acta* **2007**, *52*, 3785–3793. [CrossRef]
29. Zhao, M.; Wu, S.; An, P.; Luo, J. Study on the deterioration process of a chromium-free conversion coating on AZ91D magnesium alloy in NaCl solution. *Appl. Surf. Sci.* **2006**, *253*, 468–475. [CrossRef]